Available online at www.sciencedirect.com
ScienceDirect
Journal of Power Sources 166 (2007) 226–232
JOURNAL OF POWER SOURCES
www.elsevier.com/locate/jpowsour

# New composite polymer electrolyte comprising mesoporous lithium aluminate nanosheets and PEO/$LiClO_4$

Linfeng Hu *, Zilong Tang, Zhongtai Zhang

*State Key Laboratory of New Ceramics and Fine Processing, Department of Materials Science and Engineering, Tsinghua University, Beijing 100084, PR China*

Received 5 October 2006; received in revised form 13 January 2007; accepted 15 January 2007
Available online 20 January 2007

**Abstract**

Mesoporous materials, due to its potential for advanced applications in catalysis and nanoscience, have attracted much attention in the past decade. In this work, mesoporous lithium aluminate (next called MLA) nanosheets with high specific surface area were prepared by a hydrothermal method using hex-adecyltrimethyl ammonium bromide (CTAB) as the template. A novel PEO-based composite polymer electrolyte has been developed by using MLA powders as the filler. The electrochemical impedance showed that the conductivity was improved simultaneously. A high conductivity of $2.24 \times 10^{-5}$ S cm$^{-1}$ at 25 °C was obtained. The lithium polymer battery using this novel composite polymer electrolyte and with lithium metal and $LiFePO_4$ employed as anode and cathode, respectively, showed high discharge capacity (more than 140 mAh g$^{-1}$ at 60 °C) and excellent cycling stability as revealed by galvanostastically charge/discharge cycling tests. The excellent electrochemical performances at low temperature of the cells were obtained, which was attributed to the high surface area and channels structure of the filler. The excellent properties of the solid-state lithium battery suggested that, $PEO_{16}$–$LiClO_4$–MLA composite polymer electrolyte can be used as a candidate material for lithium polymer batteries.


*Keywords:* Mesoporous; Lithium aluminate; Composite polymer electrolyte

## 1. Introduction

There has been increasing interest in the development of polymer electrolytes, due to their applications in solid-state electrochemical devise, and particularly in solid-state rechargeable lithium aluminate [1]. Since Wright [2] found that the complex of PEO and alkaline salts had the ability of ionic conductivity in 1973, PEO–LiX-based polymer electrolytes have received extensive attentions, for its potential capability to be used as candidate material for the traditional liquid electrolytes.

A number of experiments denied the possibility of ionic conductivity in crystalline polymers [3,4]. As a result, attention for the past 30 years has concentrated on amorphous polymer electrolytes [5], and in particular on the synthesis of new materials with low crystallinity and high levels of segmental motion in order to increase the conductivity. This attention resulted two different classes of polymer electrolytes: known as gel polymer electrolyte (GPEs) and composite polymer electrolytes (CPEs) [6]. The mechanical properties and chemical stability of CPEs are much better than those of GPEs, so CPEs have better application prospects than GPEs. However, the ionic conductivity of CPEs is often lower than $10^{-6}$ S cm$^{-1}$ at room temperature. For this reason, our work is focusing on the improvement of CPEs. One of the promising method to enhance ionic conductivity is to disperse inorganic ceramic fillers into the conventional PEO–LiX system [7,8], such as $SiO_2$ [9], $TiO_2$ [10], MSCN (M = Li, Na, K) [11], $Sm_2O_3$ [12], $ZrO_2$ [13], $Al_2O_3$ [14–16], $SnO_2$ [17], $V_2O_5$ [18], layered clays (e.g. montmorillonite) [19]. Moreover, microporous molecular sieves have been added into PEO matrix as excellent fillers. Mesoporous silica, such as MCM-41, SAB-15, HMS can enhance the electrochemical properties such as ion conductivity, lithium ion transference numbers, lithium electrode interface stability and electrochemical stability markedly [20–22]. However, these mesoporous silica are neither electronically nor ionically conductive.

* Corresponding author. Tel.: +86 10 6277 2623; fax: + 86 10 6278 3046.
*E-mail address:* hlf05@mails.tsinghua.edu.cn (L. Hu).

0378-7753/$ – see front matter © 2007 Elsevier B.V. All rights reserved.
doi:10.1016/j.jpowsour.2007.01.028

Lithium aluminate ($LiAlO_2$), has been reported as a solid ionic conductor working at low temperatures investigated by means of NMR [23]. It is an effective filler in linear PEO-based polymeric electrolyte systems. The system PEO–$LiClO_4$–$LiAlO_2$ has been studied. Better mechanical properties, higher conductivity and enhanced interfacial stability with respect to PEO–$LiClO_4$ have been found [24]. Moreover, the addition of $LiAlO_2$ powders could effectively control the growth of the passivation layer on the lithium aluminate [25]. Croce has reported a kind of polymer electrolyte consisting of PEO–$LiClO_4$–$LiAlO_2$, and a high conductivity of $2.9 \times 10^{-6}$ S cm$^{-1}$ at 25 °C has been obtained [26,27]. However, the $LiAlO_2$ particle used was with the average particle of about 1–4 μm, and its surface area was very limited. We suggested that the mesoporous structural $LiAlO_2$ nanosheets may act as a better filler than conventional several μm $LiAlO_2$ particles.

In this paper, we report a novel PEO-based composite polymer electrolyte using mesoporous lithium aluminate (MLA) powders as the filler. MLA nanosheets were prepared by a simple hydrothermal method using CTAB as the template, and then were complex with $PEO_{16}$–$LiClO_4$. We observed a very large enhancement of conductivity and a high discharge capacity by addition of these electrically active MLA nanosheets. The properties of this new $PEO_{16}$–$LiClO_4$–MLA were much better than the reported results of CPEs with 4 μm $LiAlO_2$ as the filler [26,27]. The excellent performances of the cells suggested that, the novel $PEO_{16}$–$LiClO_4$–MLA electrolyte can be used as a candidate material for lithium polymer batteries.

## 2. Experiment

### 2.1. Preparation of MLA nanosheets

Mesoporous lithium aluminate nanosheets have been synthesized prepared by a simple hydrothermal route using the surfactant CTAB as the template as follows: 50 mmol distilled water was added slowly to the mixture of 100 mmol lithium hydroxide ($LiOH{\cdot}H_2O$) (A.R.), 100 mmol aluminum *iso*-propoxide (AIP) (A.R.) and 100 mmol hex-adecyltrimethyl ammonium bromide (CTAB) (A.R.). The mixture was put into a Teflon autoclave vessel. The hydrothermal reaction was followed at 120–150 °C under autogenous pressure for 10 h. The precursor was washed several times by absolute ethanol, dried at 80 °C for 10 h, and then calcined at 500 °C for 4 h in air.

### 2.2. Preparation of $PEO_{16}$–$LiClO_4$–MLA films

PEO (Alfa Aesar Co.) with average molecular weight of 300,000 was used. $LiClO_4$ (Alfa Aesar) was dried in a vacuum oven at 100 °C for 48 h and then stored in a vacuum oven. The MLA powders were heated under vacuum at 150 °C for 48 h to remove the water adsorbed in the mesopores. The composite polymer electrolyte PEO–$LiClO_4$–MLA was synthesized by the conventional solution cast technique. MLA powders ware dispersed in acetonitrile with the aid of ultrasonic dispersion, followed by the addition of PEO and $LiClO_4$ which concentration ration was fixed at 16. The solution was stirred at room temperature for 24 h until the mixture appeared to be homogeneous. Then the mixture was cast on a Teflon plate followed by evaporating solvent in an argon-filled glove box for 10 h. Finally, the samples were dried under vacuum at 80 °C for 48 h. The films obtained were 200–300 μm in thickness, approximately.

### 2.3. Characterization of samples

X-ray diffraction (XRD) patterns of samples were recorded by a Rigaku D/max-RB diffractometer with monochromatized Cu Kα radiation (λ = 1.5418 Å). A JEM-2011 transmission electron microscopy (TEM) with acceleration voltage of 200 kV and a JEOL JSM-6460LV scanning electron microscopy (SEM) were used to observe the morphology of the samples. Differential scanning calorimetry (DSC) was used to characterize the flexibility of the PEO chain and the melting heat of the polymer electrolyte by using a Dupont TA 2910 modulated DSC. The specific surface area was estimated by the Brunauer–Emmett–Teller (BET) four-points method, on the basis of the nitrogen gas adsorption isotherm (77.4 K) with a NOVA4000 high gas sorption analyzer. The pore size distribution was also analyzed with the same apparatus.

### 2.4. Measurement of electrochemical performances

The complex impedance was measured by a HP 4192A LF impedance analyzer in the frequency range from 5 Hz to 2 MHz. The composite film was sandwiched between stainless steel blocking electrodes (0.8 cm in diameter). The impedance was gauged in air over the range 25–80 °C. The bulk resistance ($R_b$) was obtained by reading the intercept of impedance spectrum [29], and the conductivity was calculated from: $\sigma = L/(R_bA)$, wherein $L$ is the thickness of the electrolyte film and $A$ represented the electrode area. The electrolyte potential stability windows were determined by linear sweep voltammetry, using stainless steel as a working electrode, lithium metal as a reference electrode and the novel CPE film as the electrolyte. CHI 660A electrochemical workstation was used for voltammetry measurement.

Solid-state lithium battery was then prepared using the novel CPE as the electrolyte. $LiFePO_4$ and lithium metal were employed as anode and cathode materials of the cells, respectively. The cells were constructed and handled in a argon-filled glove box and evaluated using coin-type cells (CR2032). Electrochemical measurement was carried out using a LAND Celltest-2001A (Wuhan, China) system. The cells were galvanostatically diacharged and charged between 4.2 and 2.5 V.

## 3. Results and discussion

### 3.1. Properties of MLA powders

Two-dimensional nanosheets exhibited in the TEM micrograph (Fig. 1a). The size of nanosheet was about 300–500 nm, and many disordered mesopores were discovered on the nanosheets. The diameter of the mesopore was 10 nm, approximately (Fig. 1a, insert). The SEM image showed that the

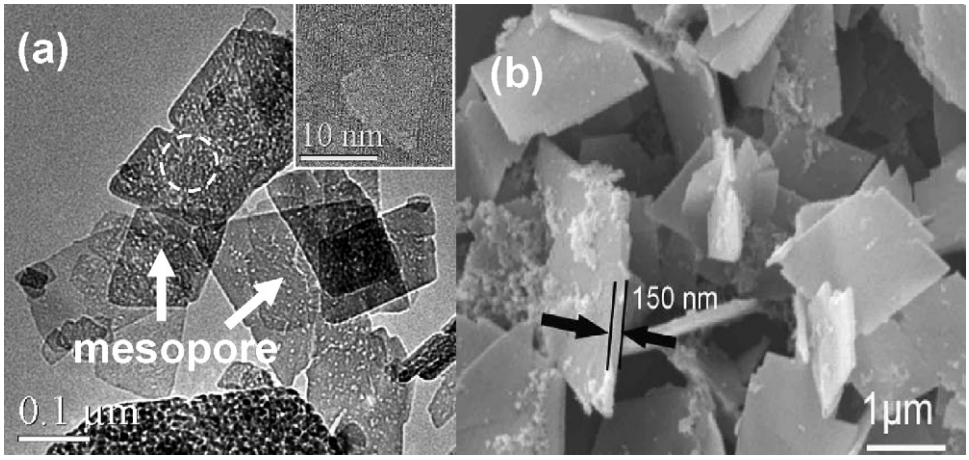


Fig. 1. (a) Typical TEM image for MLA nanosheets, with HRTEM image of mesopore inserted; (b) SEM image for MLA nanosheets.

thickness of the nanosheet was about 150 nm, so they could be called as "nanosheets".

The XRD patterns in Fig. 2 of MLA showed that it could be characterized as a hexagonal ($R\bar{3}m$) α-$LiAlO_2$ phase, with lattice constants $a = 2.800$ Å and $c = 14.21$ Å (JCPDS No. 74-2232). The small angle diffraction patterns inserted in Fig. 2 did not show any resolved diffraction peak, which implied absence of mesostructure order in the pore arrangement for the MLA nanosheets. This result was corresponding to the TEM observation. Specific surface area of the products was calculated according to nitrogen adsorption measurements. The specific surface area of MLA was 124 $m^2\,g^{-1}$. The isotherm of nitrogen adsorption and desorption in Fig. 3 demonstrated the typical diffusion bottleneck structure, which exhibited large hysteresis loop of type IV with sloping adsorption branch and steep desorption branch. The hysteresis type was due to the presence of different size of spheroidal cavities with the same entrance pore diameter. Pore size distribution which was determined by the Brunauer–Joyner–Halenda (BJH) method from the desorption loop showed a narrow range of 2.82 nm (Fig. 3, inserted).

### 3.2. Properties of polymer electrolyte $PEO_{16}$–$LiClO_4$–MLA

Fig. 4 displayed the crystallinity change in the composite polymer electrolyte $PEO_{16}$–$LiClO_4$–$x$ wt% MLA by X-ray diffraction. The characteristic diffraction peaks of crystalline PEO were apparent between $2\theta = 19°$ and 23.5°. However, these diffraction peaks became broader and less prominent in the $PEO_{16}$–$LiClO_4$–$x$ wt% MLA complex films. The peaks characteristic intensities were decreased further with lowest intensity reached in between 12 and 15 wt%. The results affirmed the addition of MLA powders could decrease the crystallinity of PEO effectively.

DSC thermograms of PEO, $PEO_{16}$–$LiClO_4$, and $PEO_{16}$–$LiClO_4$–$x$ wt% MLA were displayed in Fig. 5. The relative percentage of crystallinity ($\chi_c$) has been calculated by taking pure PEO as 100% crystalline and using the equation $\chi = \Delta H_f / \Delta H_f^0$ (the heat enthalpy of 100% crystalline PEO is 203 $J\,g^{-1}$ [28]). The calculated relative crystallinity $\chi$ and the data obtained from DSC curves and were summarized in Table 1. The melting temperature ($T_m$) of crysyalline PEO

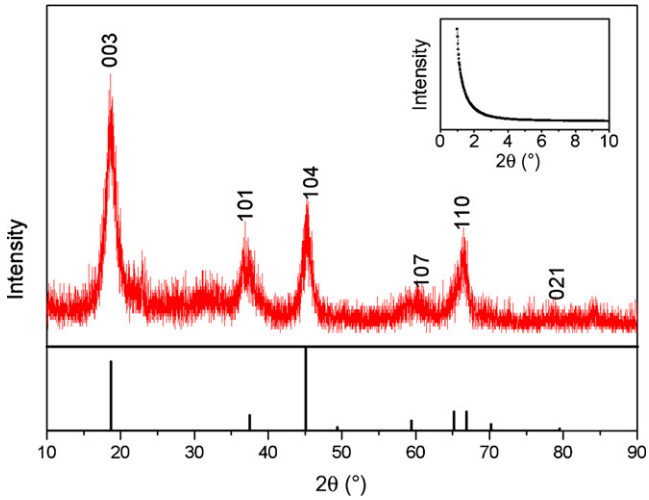


Fig. 2. Wide-angle and small angle XRD patterns of mesoporous lithium aluminate.

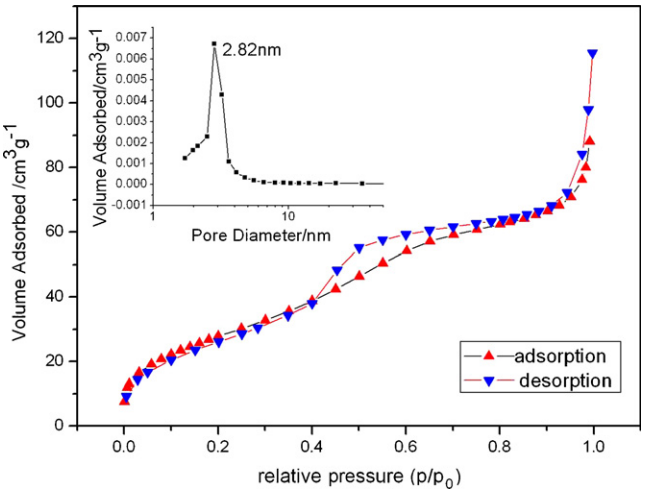


Fig. 3. Nitrogen adsorption–desorption isotherms and pore size distribution of the mesoporous lithium aluminate powders.

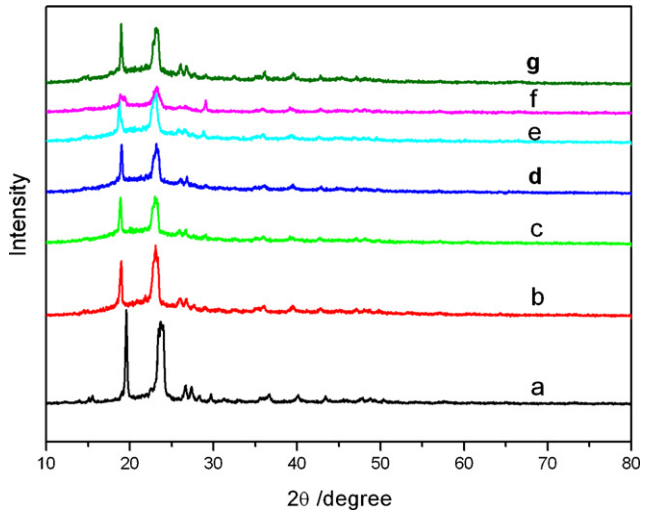


Fig. 4. X-ray diffraction patterns of: (a) pure PEO, and $PEO_{16}$–$LiClO_4$ with MLA of different weigh ratios: (b) 0%, (c) 5%, (d) 10%, (e) 12%, (f) 15%, (g) 20%.

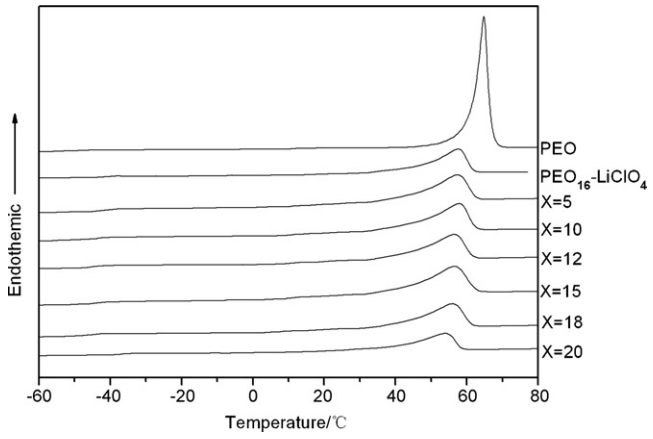


Fig. 5. The DSC curves of pure PEO, $PEO_{16}$–$LiClO_4$, and $PEO_{16}$–$LiClO_4$–*x* wt% MLA.

phase decreased from 57.6 to 54.0 °C when the content of MLA increased from 0 to 20 wt%. The glass transition temperature, $T_g$, of PEO also decreased with the addition of MLA. The decrease of $T_g$ and $\chi_c$ indicated that, the addition of MLA could increase the flexibility of PEO chains and the ratio of amorphous PEO, respectively. Both XRD and DSC studies indicated that PEO crystallinity was deteriorated by the lithium salt and further by the addition of MAL powders. Consequently, ionic conductivity should be enhanced at low temperature.

Table 1
DSC results for $PEO_{16}$–$LiClO_4$–MLA composite electrolytes

| wt% of MLA | $T_g$ (°C) | $T_m$ (°C) | $\Delta H_m$ (J g$^{-1}$) | $\chi_c$ (%) |
|---|---|---|---|---|
| 0 (pure PEO) | −51.9 | 64.8 | 113.4 | 55.86 |
| 0 | −40.9 | 57.6 | 64.3 | 31.7 |
| 5 | −40.4 | 57.3 | 61.7 | 30.4 |
| 10 | −42.7 | 57.7 | 59.7 | 29.4 |
| 12 | −44.2 | 56.4 | 56.8 | 28.0 |
| 15 | −43.7 | 56.5 | 56.7 | 27.9 |
| 18 | −45.8 | 56.0 | 55.2 | 27.2 |
| 20 | −45.7 | 54.0 | 53.1 | 26.1 |

Scanning electron micrographs of pure PEO and $PEO_{16}$–$LiClO_4$–MLA films were displayed in Fig. 5. The micrograph for pure PEO showed a rough surface which had several crystalline domains. Some micro-cracks were found on the surface. On blending with lithium salt, the surface morphology was changed obviously. Fig. 5 showed a dramatic improvement of surface morphology from rough to smooth. The smooth morphology was closely related to the reduction of PEO crystalline. We could see that the crystalline domains were still present but became much smaller than the pure PEO. From the high magnification of $PEO_{16}$–$LiClO_4$–15 wt% MLA, the mesoporous nanosheets could be observed clearly, which demonstrated that MLA could maintain its nanosheet structure in the composite polymer electrolytes. MLA nanosheets were homogeneously dispersed in the matrix, which was implied by the space distribution of Al element in the polymer electrolyte films of $PEO_{16}$–$LiClO_4$–15 wt% MLA (Fig. 6).

The temperature dependence of ionic conductivity of $PEO_{16}$–$LiClO_4$–MLA was displayed in Fig. 7. The overall features of the Arrhenius plots were similar for all these composite films. All the curves had a turning point around 55–60 °C, corresponding to the transition from the crystalline state of PEO to the amorphous phase. The introduction of MLA powders had a significant effect on the ionic conductivity of CPE. The enhancement of ionic conductivity was most pronounced at low temperature. Ionic conductivity first increased sharply with MLA content and reached at the maximum value that was about $2.24 \times 10^{-5}$ S cm$^{-1}$ at 25 °C by 15 wt% loading content of MLA. This value was about more than 100 times higher than the pristine $PEO_{16}$–$LiClO_4$ (Fig. 8). When MLA content increased further, ionic conductivity decreased. Decreasing of the ionic conductivity was attributed to the blocking effect on the transport of charge carriers, resulting from the aggregating of the MLA nanosheets.

Fig. 9 displayed the liner linear voltage sweep curves of $PEO_{16}$–$LiClO_4$–15 wt% MLA composite electrolyte. The sample exhibited good electrochemical stability up to 5.0 V. Moreover, the results proved that the peak area decreased after the addition of MLA, suggesting that MLA nanosheets could absorb the residual solvents in the CPE effectively, which was beneficial for keeping the stability of the interface between CPE and lithium metal electrolyte. This result was the same with the observation of Xi et al. [29]. The good electrochemical stability suggested that, this composite polymer could be used as a candidate electrolyte material for rechargeable lithium polymer batteries whose working voltage was higher than 4.5 V.

The cycle ability of the cell using the composite polymer electrolyte was measured at 0.1–0.5*C* at 60 °C. It was obvious that the cell achieved a high capacity of 140, 130, 120 mAh g$^{-1}$ at discharge/charge rate of 0.1*C*, 0.2*C*, 0.5*C* respectively. The charge and discharge capacity and coulombic efficiency of the cells as a function of cycle number were presented in Fig. 10. The charge capacity of the cell showed no changes as the cycle number increased and the discharge/charge rate enhanced. In the first cycle, the coulombic was only 85%, after the initial first

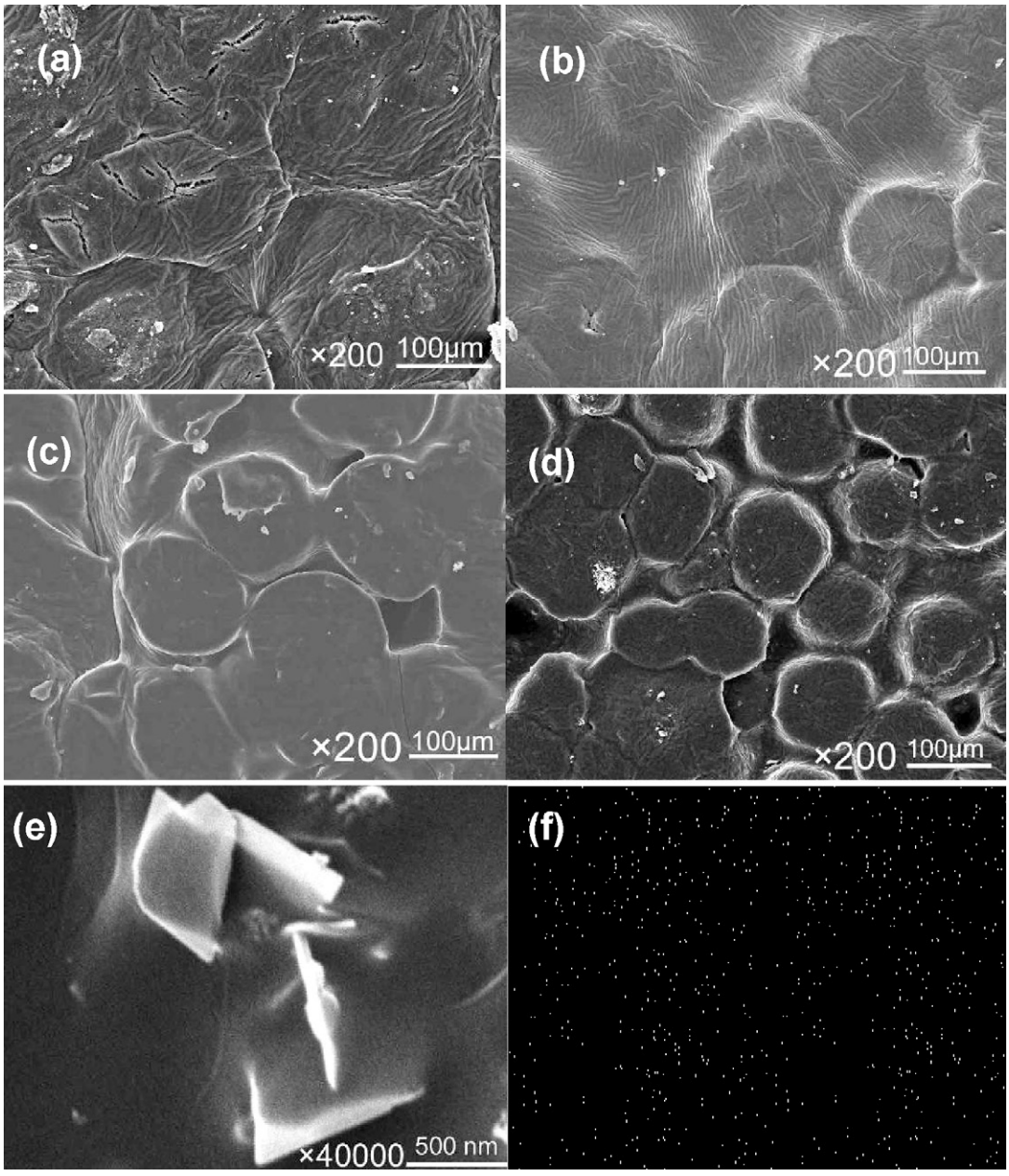


Fig. 6. SEM images of pure PEO (a), $PEO_{16}$–$LiClO_4$ (b), and $PEO_{16}$–$LiClO_4$–$x$ wt% MLA: (c) $x = 5$; (d) $x = 15$; (e) high magnification SEM image for $x = 15$; (f) the space distribution of Al element in the polymer electrolyte films.

cycle it was estimated to more than 93%. The large irreversible capacity observed in the first cycle could be ascribed to an initial poor interfacial contract between the polymer electrolyte film and $LiFeO_4$ electrode. When changing the charge/discharge current density, the capacity still could keep stable to a corresponding level. Fig. 11 demonstrated that these cycles had a coulombic efficiency approaching 100% even at very high rates. This novel $PEO_{16}$–$LiClO_4$–15 wt% MLA composite polymer electrolyte could be used at 60 °C low temperature. To the best of our knowledge, it was one of the lowest values of active temperature as far as reported for composite PEO-based polymer electrolyte lithium batteries [30,31]. The high charge/discharge capacity and excellent cycling stability at low temperature suggested that, this novel polymer electrolyte could be used as a candidate material for lithium polymer batteries. However, when discharge/charge rate raise to 1.0*C*, a capacity degradation to 80 mAh $g^{-1}$ was observed. At present, these tests are still in progress with the capacity degradation.

Fig. 12 presented the schematic presentation of $PEO_{16}$–$LiClO_4$–MLA composite polymer electrolyte. There may be no Lewis base on the surface of MLA nanosheet, so it cannot cause and competition mechanism and ion pair dissociation for $LiClO_4$ as Croce reported [26]. The lithium ion path through ceramic filler is not available, which is reported in Abe's work [32]. However, as MLA is the mesoporous filler, lithium ion could path through the channels of mesopores, which has been proved by Xi et al. [20]. So MLA powders may enhance the lithium ionic conductivity through three

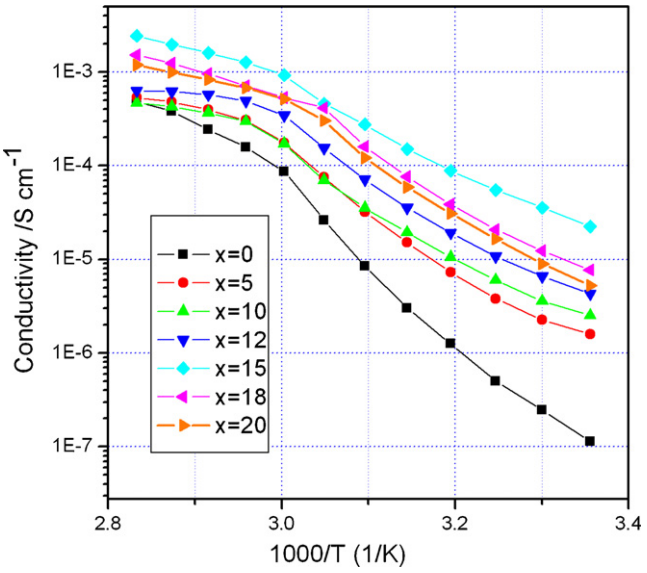


Fig. 7. Temperature dependence of ionic conductivity of $PEO_{16}$–$LiClO_4$–$x$ wt% MLA composite polymer electrolytes.

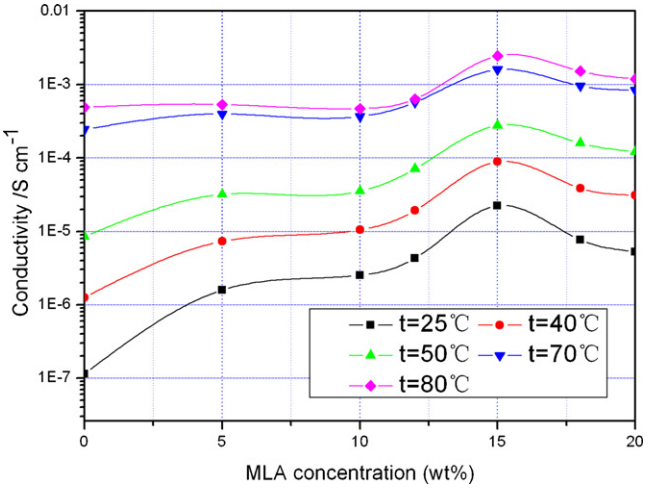


Fig. 8. Dependence of the ionic conductivity of the $PEO_{16}$–$LiClO_4$–MLA composite electrolytes on MLA concentration (wt%) at different temperatures.

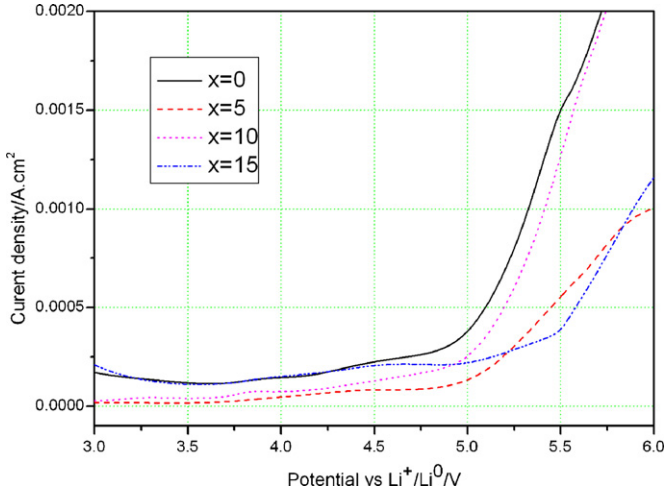


Fig. 9. Current–voltage response of $PEO_{16}$–$LiClO_4$–$x$ wt% MLA composite polymer electrolyte at 60 °C on stainless steel electrode as a working electrode: $x = 0$, 5, 10, 15 (scanning rate: 10 mV $s^{-1}$).

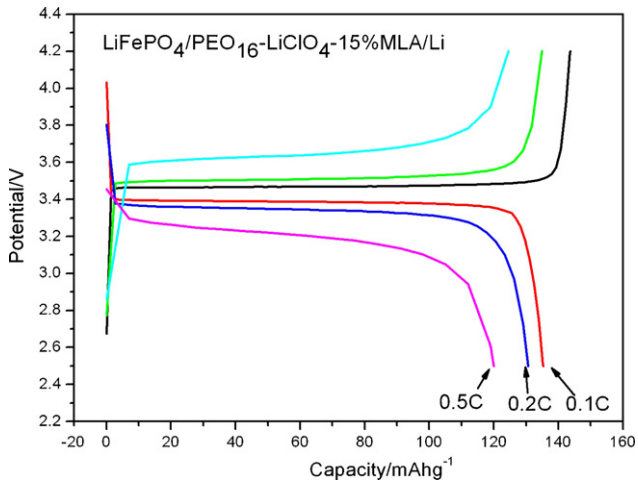


Fig. 10. The charge–discharge performance of Li $FePO_4$/$PEO_{16}$–$LiClO_4$–15 wt% MLA/Li cell at 60 °C with different discharge/charge rates.

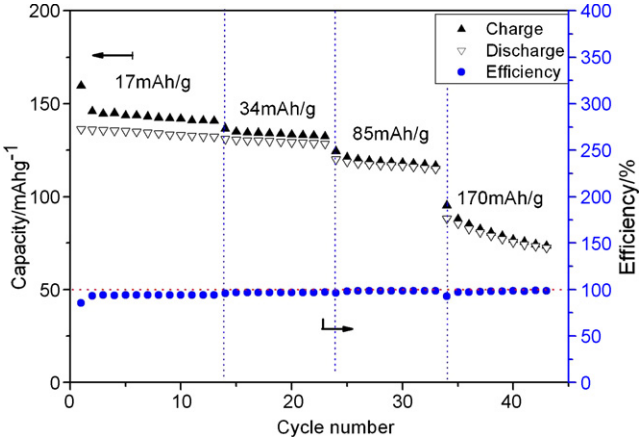


Fig. 11. Charge and discharge capacity cycling performance and the coulombic efficiency of Li/$PEO_{16}$–$LiClO_4$–15 wt% MLA/$LiFePO_4$ battery at various current densities.

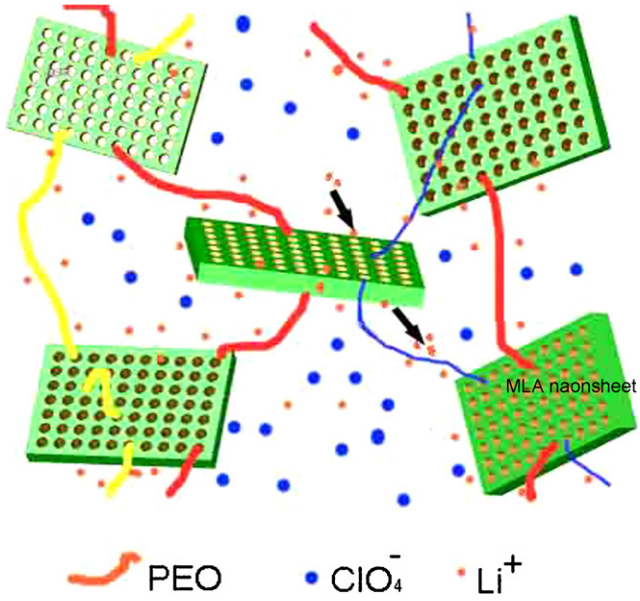


Fig. 12. Schematic respresentation of $PEO_{16}$–$LiClO_4$–MLA composite polymer electrolyte.

ways: (1) prevent the reorganization of PEO chains which have intercalated into its mesoporous channels, which has been elucidated by XRD and DSC datas. Since the MLA channel is relatively huge (2.8 nm), it is possible that the PEO chains are permeated into the mesopores, and thus the MLA particles mat act as physical cross-linking centers for PEO chains; (2) the high specific surface area of MLA leads to a higher interfacial area between the polymer and the fillers. Lithium ion can transport through the surface of MLA nanosheets, thereby it leads to a further increase in the ionic conductivity; (3) selective passing of $Li^+$ cation due to the special pore size and channel structures of MLA. The charge transport through the nanochannels of MLA provides a fast conduction path. As the ionic diameters of $Li^+$ and $ClO_4^-$ are 0.152 and 0.474 nm, respectively, and the pore size of MLA was 2.8 nm, $Li^+$ can enter and path through the channels and pores in MLA nanosheets more easily than $ClO_4^-$.

The lithium ion may conduct as two different mechanisms. The fundamental ion transport is achieved by random walking through amorphous PEO chains. The second conduction path is established by lithium ion hopping in sequential manner on the interior mesoporous channels and exterior surface of the nanosheets. The bulk temperature-dependent conductivity is the average of temperature-dependent conductivities of these two lithium conductions. The favorable conductivity behavior of the CPE containing the active MLA nanosheets are attributed to the combined effect of suppressing PEO crystallinity, higher interface area between the fillers and polymer matrix, and existence of such a new type of channel conducting mechanism. For these reasons, the $PEO_{16}$–$LiClO_4$–MLA composite polymer electrolyte showed higher conductivity and better electrochemical performances than those several μm $LiAlO_2$ particles.

## 4. Conclusions

In summary, a novel PEO-based composite polymer electrolyte has been developed by using mesoporous lithium aluminate (MLA) nanosheets as the filler, which were successfully synthesized through a simple hydrothermal route. The MLA nanosheets served as excellent fillers to polymer electrolyte composing PEO and $LiClO_4$ for its high specific surface area and mesoporous structure. Compared with the 1–4 μm γ-$LiAlO_2$ particle [27], it is a better addition agent into polymeric electrolyte of lithium secondary battery to enhance the ionic conductivity. The increased conductivity of the new composite polymer electrolyte reached a maximum of $2.24 \times 10^{-5}$ S cm$^{-1}$ at 25 °C, which was more than two order higher than that without MLA fillers. The optimum value of the MLA loading was found at 15 wt%. These polymer electrolytes exhibited good electrochemical stability up to 5.0 V. The lithium polymer battery using this novel composite polymer electrolyte showed high discharge capacity of 140 mAh g$^{-1}$ at 60 °C.

## Acknowledgments

Authors gratefully acknowledge the support of National Natural Science Funds of China (Grant Nos. 50472005 and 50372033), as well as the Basic Research Funds of Tsinghua University (Grant No. JC 2003040).

## References

[1] J.M. Tarascon, M. Armand, Nature 414 (2001) 359.
[2] D.E. Fenton, J.M. Parker, P.V. Wright, Polymer 14 (1973) 589.
[3] Z. Stoeva, I. Martin-Litas, E. Staunton, et al., J. Am. Chem. Soc. 125 (2003) 4619.
[4] E. Staunton, G.A. Yuri, P.G. Bruce, J. Am. Chem. Soc 127 (2005) 12176.
[5] F. Croce, R. Curini, A. Martinelli, L. Persi, et al., J. Phys. Chem. B. 103 (1999) 10632.
[6] A.M. Christie, S.J. Lilley, P.G. Bruce, Nature 43 (2005) 352.
[7] L.M. Bronstein, C. Joo, R. Karlinsey, et al., Chem. Mater. 13 (2001) 3678.
[8] R.L. Edson, L.S. Flavio, R.B. Paulo, et al., Chem. Mater. 17 (2005) 4561.
[9] J. Kim, K. Ji, J. Lee, et al., J. Power Sources 119 (2003) 415.
[10] F. Corce, G.B. Appetecchi, L. Persi, Nature 394 (1998) 456.
[11] A. Zalewska, J. Stygar, E. Ciszewska, et al., J. Phys. Chem. B 105 (2001) 5847.
[12] P.P. Chu, M.J. Reddy, J. Power Sources 115 (2003) 288.
[13] F. Crose, L. Settimi, B. Scrosati, Electrochem. Commun. 8 (2006) 364.
[14] Y.W.C. Yang, S.Y. Chen, et al., Macromolecules 38 (2005) 2710.
[15] Z.X. Wang, X.J. Huang, L.Q. Chen, Electrochem. Solid State Lett. 6 (2003) 40.
[16] H.M. Xiong, K.K. Zhao, X. Zhao, Solid State Ionics 159 (2003) 89.
[17] B. Juraj, H. Emily, P.G. Emmanuel, Chem. Mater. 12 (2000) 2168.
[18] M.K. Grant, A.T. Joyce, W.B. Paul, et al., Chem. Mater. 8 (1996) 2418.
[19] L.Z. Fan, C.W. Nan, M. Li, Chem. Phys. Lett. 369 (2003) 698.
[20] J.Y. Xi, S.J. Mao, X.Z. Tang, Macromolecules 37 (2004) 8592.
[21] J.Y. Xi, X.P. Qin, W.T. Zhu, Micropor. Mesopor. Mater. 88 (2006) 7.
[22] C.W. Nan, L.Z. Fan, Y.H. Lin, Phys. Rev. Lett. 91 (2003) 266104.
[23] H.J. Kim, H.C. Lee, C.H. Khee, J. Am. Chem. Soc. 125 (2003) 13354.
[24] F. Croce, B. Scrosati, G. Mariotto, Chem. Mater. 4 (1992) 134.
[25] B. Scrosati, F. Croce, J. Power Sources 9 (1993) 43.
[26] F. Croce, L. Persi, F. Ronci, Solid State Ionics 135 (2000) 47.
[27] W. Gang, F. Croce, B. Scrosati, Solid State Ionics 53–56 (1992) 1102; P.P. Chu, M.J. Reddy, H.M. Kao, Solid State Ionics 156 (2003) 143.
[28] B. Wiunderlich, Macromolecular Physics, vol. 3, Academic Press, New York, 1980, p. 67.
[29] J.Y. Xi, X.P. Qiu, L.Q. Chen, Solid State Ionics 176 (2005) 1249.
[30] F. Croce, F.S. Fiory, L. Persi, Electrochem. Solid State Lett. 4 (2001) A121.
[31] Y. Matoba, S. Matsui, M. Tabuchi, et al., J. Power Sources 137 (2004) 284.
[32] T. Abe, F. Sagane, M. Ohtsuka, et al., J. Electrochem. Soc. 151 (11) (2004) A1950.